Method for Measurement of Photon Incident Angle in CsI Calorimeter

Ivan Teo

20 May 2009

Abstract

The recent development of a timing instrument accurate to 100 picoseconds may enable the CsI calorimeter in the E14 experiment to measure the incident angle of incoming photons, a feat that E14's predecessor E391a, was unable to accomplish. Consequently, the $K_L^0 \to \pi^0 \nu \overline{\nu}$ decay, otherwise known as the "golden mode" decay, can be more reliably identified and counted. Using a Monte Carlo simulation, we present a method utilizing the new timing instrument to measure the incident angle of a photon to 10° or less accuracy along one dimension.

I would like to thank, first and foremost, my adviser Prof. Yau Wah for his guidance and the numerous pointers that have gotten me past dead-ends in the course of this work. I thank also Professors Gene Mazenko and Margaret Gardel for their useful suggestions on writing this paper and for overseeing the senior thesis program. Last but not least, my colleague Jiasen Ma has my gratitude for helping me to understand PAW and GEANT, and for deftly solving the occasional programming problem.

1 Introduction

1.1 Branching Ratio of the Golden Mode Decay

The theoretical value of the $K_L^0 \to \pi^0 \nu\bar{\nu}$ decay branching ratio is calculated to be $(2.6 \pm 0.3) \times 10^{-11}$ [1] by incorporating CP violation in the Standard Model. The experimental determination of this branching ratio can be said to be an ideal test of CP violation owing to the small uncertainty in its theoretical value.

1.2 Overview of E14

The aim of the E14 experiment is to measure the golden mode branching ratio. E14's predecessor, E391a, had the same general setup. It counted the number of golden mode decays occurring within a large sample of kaon decays ($(5.13 \pm 0.4) \times 10^9$), giving a branching ratio value of 6.7×10^{-8} at 90% CL.[2]

In the experiment, a 12GeV proton beam is incident on a Pt target, producing a beam that contains, but does not purely consist of, K_L^0 particles. (Figure 1) The methods employed to distinguish between K_L^0 and background are beyond the scope of this project.

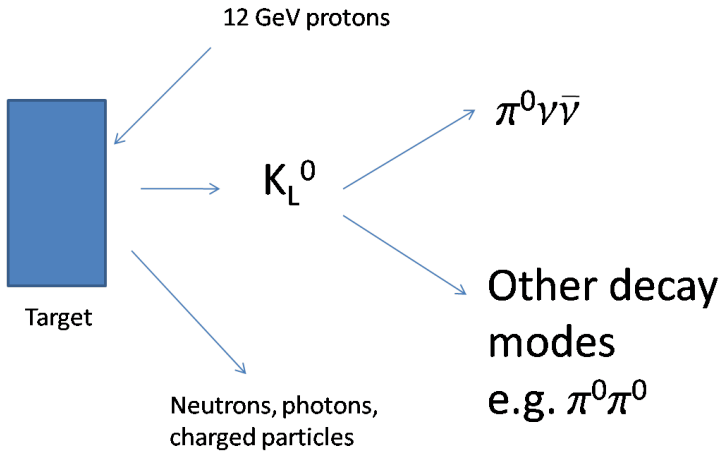

Figure 1

The beam is channeled into the fiducial decay region in the detector where kaon decay occurs. Event rejection is effected by veto calorimeters to detect stray photons. The details of this process are also outside the scope of this project. The CsI calorimeter is used to reconstruct the accepted events from decay products, namely photons, incident on it.

1.3 Identifying Golden Mode Decays

The main challenge in the experiment is signal definition, which must be very sensitive due to the extremely small branching ratio of the decay. The golden

mode decay produces a π^0 and $\nu\overline{\nu}$. The neutrino and antineutrino are too difficult to detect, and hence do not enter into consideration for signal definition. The π^0 further decays into two photons with a high branching fraction of $\sim$ 98.8%. (Figure 2) These photons must be collected by the CsI calorimeter because the time and energy information obtained from them is required to apply kinematic cuts. Hence we require that two photons for each π^0 be incident on the CsI calorimeter with no collection on the veto calorimeters.

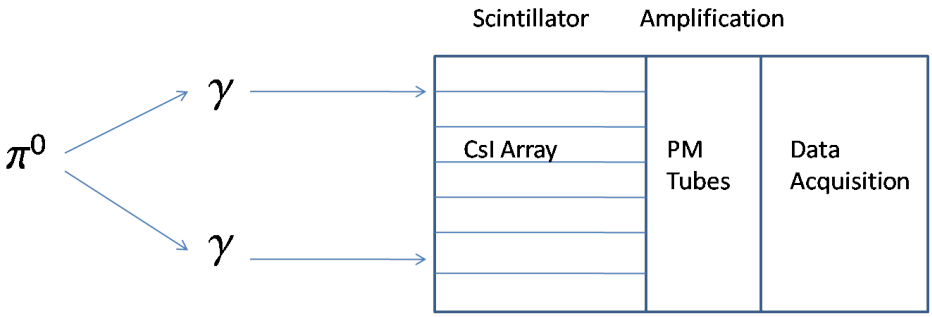

Figure 2

The above criterion is insufficient. A complete kinematic description would also require that a collected pair of photons did indeed come from a π^0. Namely, we require that the photons be kinematically consistent with a π^0.

1.4 Kinematic Consistency and the Importance of Photon Incident Angle

Solving the equations for conservation of energy, linear momentum and 4-vectors would allow us to reconstruct the π^0. Using subscripts π for the pion (supposed) and $\gamma 1$ and $\gamma 2$ for the two photons in the energy E, rest mass m and momentum P, these equations are:

$$\begin{gathered} E_\pi = E_{\gamma 1} + E_{\gamma 2} \\ P_{\pi i} = P_{\gamma 1 i} + P_{\gamma 2 i}, i = x, y, z \\ E_{\gamma 1}^2 - P_{\gamma 1}^2 = 0 \\ E_{\gamma 2}^2 - P_{\gamma 2}^2 = 0 \\ E_\pi^2 - P_\pi^2 = m_\pi^2 \end{gathered}$$

These are 7 equations in 12 unknowns. Measuring the photon energies would give another 2 equations, which are not enough to solve for all the unknowns. In contrast, measuring the photon momenta components along each direction would give 6 more equations, which enables us to solve for all the unknowns. Algebraic manipulation of the above equations give us

$$2E_{\gamma 1}E_{\gamma 2}(1 - \cos\theta_0) = m_\pi^2$$

where θ_0 is the angle between the direction of propagation of both photons. We can measure $E_{\gamma 1}$ and $E_{\gamma 2}$, and obtain θ_0 by measuring the incidence angle of each photon. The resulting value of m_π must match the accepted literature value for the π^0 mass for us to conclude that the photons are indeed decay products of the π^0.

In event reconstruction, the vertex of the π^0 decay is also of interest to us. This can be obtained by measuring the photon incidence angles and the distance between the sites on which the photons are incident.

1.5 Purpose and Overview of the Project

The purpose of this project is to study the feasibility of measuring photon incident angle with the new timing instrument, assuming a photon energy of 1GeV. More specifically, we want to find an application of kinematic fitting [3] to measure photon incident angle using time data collected by the detector.

We use Monte Carlo simulations of the detector setup to generate the data corresponding to several values of the incident angle. The data is then analyzed to find suitable fitting parameters for our purpose. The simulations are run on version 3.21 of GEANT, a CERN-developed, Fortran-based application that simulates the geometry and material of detectors and the passage of elementary particles through them. [4]

The CsI calorimeter in the E14 experiment will use a scintillator composed of an array of CsI crystals. A photon incident on the array produces an electromagnetic shower that is converted into a current pulse by the PM tube attached to each crystal. In each crystal, the energy corresponding to the current, as well as the time taken for the accumulated energy to cross a preset threshold of 1MeV, can be measured.

We use the data collected to construct a template of means and standard deviations obtained from large samples of simulated events. We now discuss this process in greater detail.

2 Method

2.1 Monte Carlo Setup

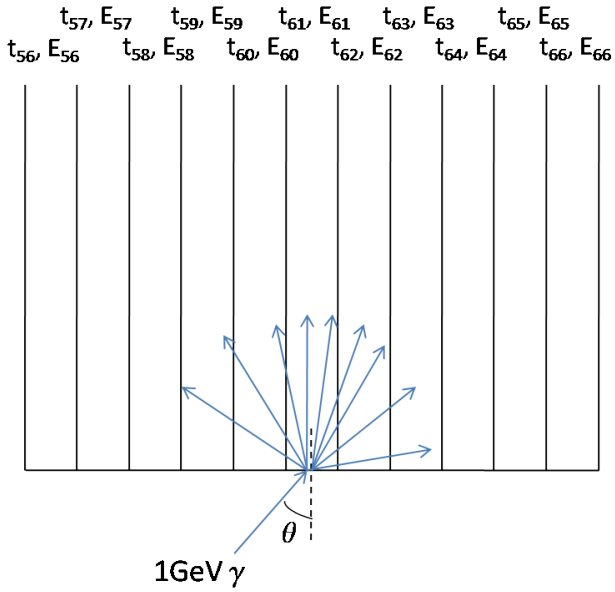

Figure 3

GEANT is used to simulate an 11×11 CsI crystal array. Each crystal has a length of 50cm with an exposed face of 2.5cm×2.5cm. The blocks are labelled 1 to 121, from left to right of each row, then from the top row downwards. Thus, the center row consists of crystal blocks 56 to 66. An incoming photon is incident at a known angle θ to the normal on the center of block 61 in the plane containing the lengths of blocks 56 to 66. For every block b, the total deposited energy E_b in block b is recorded. Also recorded is t_b, the time elapsed between the photon's generation at a fixed point in space and the crossing of the 1MeV threshold in block b. If the 1MeV threshold is not crossed, then t_b is not recorded. This constitutes one event. 5×10^4 events are simulated for each of angle $\theta = 0°$, $5°$, $10°$, $15°$, $20°$, $25°$, $30°$.

Our choice of angular range is justified by another Monte Carlo study of incident angles of photons generated by various decay processes in the experiment. Shown below are histograms of events binned by photon incident angle. Note that the incident angle generally falls between $0°$ and $30°$.

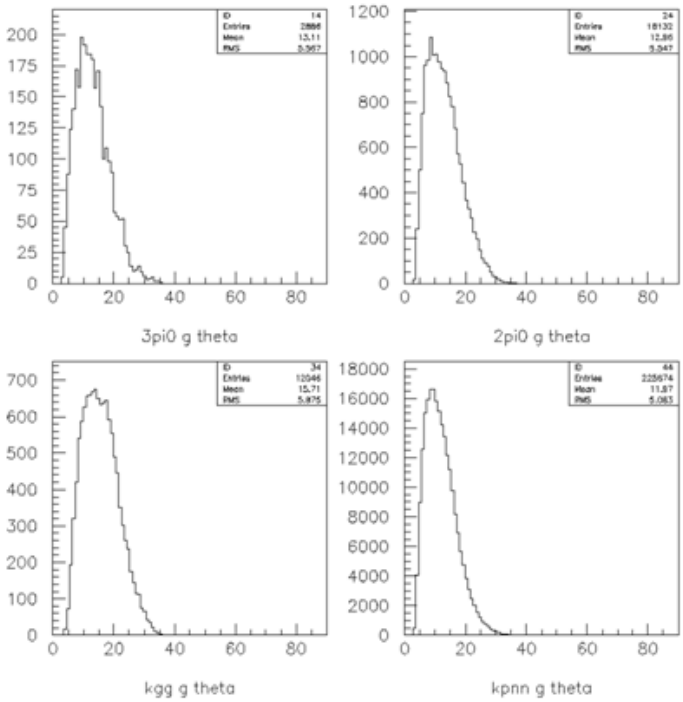

Figure 4

2.2 Histogramming and Fitting Procedure

However, not every block receives more than 1MeV of energy. This limits the number of blocks from which we can obtain information. To study the amount of information available when using 1MeV as the threshold, we histogram events for each θ by the number of blocks along the center row with $>$ 1MeV accumulated energy. These histograms are listed in Annex A. The results show that we can use, on average, between 5 to 6 blocks' data for our analysis. These blocks are about half of all the blocks in the center row. This was expected since most of the energy in the photon would be deposited in the half of the row that is in the direction of photon incidence. As far as availability of information is concerned, the choice of 1MeV for the threshold is justified.

For each event, the normalized time $\Delta t_b = t_b - t_{61}$ is calculated. Given θ and b, we expect every Δt_b to be an independent random variable with the same mean and variance, because the photon in each event sees the same detector geometry. (This assumption proves to be flawed, as we will see later.) By the Central Limit Theorem [5], the Δt_b values of each θ and b will be approximately Gaussian distributed.

Events with nonnegative t_b and t_{61} are histogrammed by Δt_b value. We obtain each histogram and the corresponding Gaussian fit as follows:
1. Build an initial histogram using an arbitrary but reasonable bin width. Use

the standard deviation of the Gaussian fit of the histogram as an estimate of the actual standard deviation.
2. Apply Scott's formula [6]:

$$W = 3.49\sigma N^{-1/3} \tag{1}$$

where W is the optimal bin width, N is the sample size, and σ is the actual standard deviation (for which we use the sample standard deviation as an estimate).

Scott's formula estimates the bin width that minimizes the integrated mean squared error of the fitted curve relative to the actual curve. Although the formula assumes the actual curve to be a Gaussian, it has been reported that calculated bin widths for skewed Gaussian do not deviate more than 30% from the optimal bin widths. Hence we do not expect the mean and variance of the fitted curve to differ significantly from those of the optimal curve. This was verified by varying the bin width within the reported error range and checking the corresponding means and variances. (Here we define significance as a change in mean of the same or greater order than the standard deviation, and/or a change in variance of order equal to or greater than the leading decimal point.)
3. A Gaussian fit is applied to the positive Δt_b region of the histogram to obtain rough estimates of the mean and standard deviation. A second Gaussian fit is then applied to the region within one standard deviation of the mean to obtain more precise values for the mean ,$\mu_b(\theta)$, and standard deviation, $\sigma_b(\theta)$.

2.3 The Anomalous Peaks Problem

Shown below for example is the histogram for $b = 63$ and $\theta = 15°$:

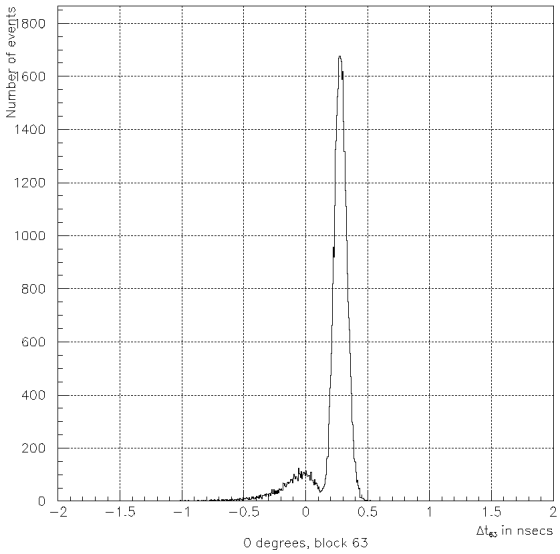

Figure 5

The reader may have spotted a problem in the above histogram. Besides the main peak, there is a smaller peak occurring mostly in the region $\Delta t_b < 0$. Similar peaks are found in the histograms for other values of θ. Only histograms for which $\theta = 0^\circ$ do not have these smaller peaks.

These anomalous $\Delta t_b < 0$ peaks present serious problems. 1) Had the anomalous peaks of different θ values been distinct from one another, we may still distinguish between two anomalous events that occur at different θ values. This was not the case as the anomalous peaks for different θ occur over the same range of Δt_b values. 2) Application of our proposed method in the actual experiment hinges on our ability to identify the block on which the photon is first incident, henceforth called the block of incidence. We have just found that the block of incidence is not the block with the smallest t_b. Hence we need to either find another way of identifying the block of incidence or abandon it as the reference block.

2.4 Explaining the Anomalous Peaks

Before we attempt to solve the problems presented above, we should understand how the anomalous peaks arise. At 1GeV, the cross-section for pair production in CsI dominates. Hence, we assume that the photon interacts only by pair production.

The attenuation of high-energy photons of intensity I_0 by pair production in an absorber of thickness x and radiation length X_0 is given by [7]:

$$I = I_0 \exp\left(-\frac{7x}{9X_0}\right)$$

The above expression says that the intensity is reduced by a factor of e when the beam travels through the distance $9X_0/7$, known as the conversion length. We may interpret this as the average distance in the absorber travelled by the photon before interacting.

In our case, the absorber is CsI and has $X_0 = 1.86$cm[8]. Hence the conversion length is 2.39cm. Now, suppose a 1GeV photon is incident at angle θ on the center of block 61. The distance travelled by the photon in block 61, if it does not interact, is OA in the diagram below, given by $OA(\theta) = 1.25/\sin\theta$.

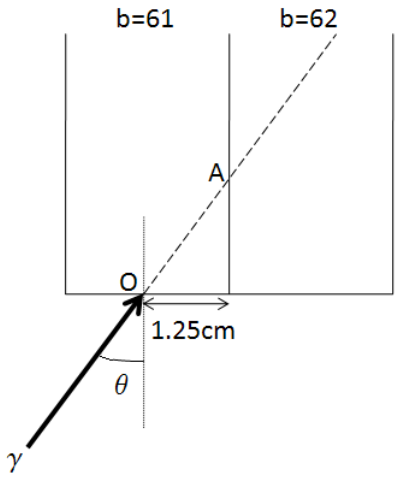

Figure 6

For some angles in the range we are interested in, $OA(5°) = 14.3$cm, $OA(10°) = 7.20$cm, $OA(15°) = 4.83$cm, $OA(20°) = 3.65$cm, $OA(25°) = 2.96$cm, $OA(30°) = 2.50$cm. Observe that the conversion length is significant compared to these lengths, especially at larger angles.

In such events, it would not be unusual to have the energy accumulated in block 62 cross the 1MeV threshold sooner than it does in block 61. This results in $\Delta t_{62} < 0$. For the larger incidence angles, we may even have $\Delta t_b < 0$ for $b > 62$. The reader is cautioned not to conclude that all late conversion events are identified with $\Delta t_b < 0$. Note that the anomalous peak extends into the $\Delta t_b > 0$ region for many of the graphs.

On a sidenote, the late conversion problem also puts our assumption that each random variable Δt_b has the same mean and variance into question. We cannot expect photons undergoing conversion nearer the next block to take the same mean amount of time to deposit energy in the next block as photons undergoing conversion further away. Indeed, we find that some of the histograms exhibit not just a second peak but also a tail on the major peak.

2.5 Re-defining Reference Block as a Solution to Late Conversion

More urgently, we would like to be able to identify the reference block for the normalization of our fitting parameters, partly because we need to offset the effect of late conversion by shifting the reference block, and also because we will not have the luxury of knowing which block to label as the block of incidence in the actual experiment.

Therefore, we abandon the use of the block of incidence for the reference. Instead, we take as our reference the block with minimum time taken for the energy to accumulate past the 1MeV threshold. The motivation for this is that the block in which the vertex of conversion occurs is intuitively likely to be the

block with the most rapid accumulation of energy. Shown below is a table of percentage of events with minimum time taken for cumulative energy deposition to cross the 1MeV threshold.

Table 1: Distribution of events by block with minimum t_b

$\theta(^\circ)$	Percentage of events with min t_b in b=				
	61	62	63	64	65
5	87.17%	10.85%	1.13%	0.23%	0.03%
10	86.81%	12.57%	0.52%	0.07%	0.01%
15	79.37%	19.31%	0.63%	0.03%	0
20	71.43%	23.74%	1.06%	0.02%	0
25	64.71%	24.20%	1.24%	0.05%	0
30	59.31%	21.40%	1.10%	0.04%	0

Note that t_b is minimum primarily in blocks 61 and 62. This is consistent with our observation that the conversion length is still within the confines of block 61 for all angles.

3 Constructing the Template

Applying the minimum time definition of reference block, we re-define $\Delta t_b = t_b - t_{min}$ where t_{min} is the time measurement in the block with the least time taken for accumulated energy to cross the threshold and b is the number of blocks to the right the current block is from the minimum time block. The resulting histograms are listed in Annex B.

If, as we suspect, the anomalous peaks are due to a shift in the vertex of conversion to the minimum time block, then the new definition will offset the shift so that Δt_b would depend only on the photon incident angle, as we originally intended. In this case, we would observe only one peak, which is true of the histograms of Δt_b. As an example, the histograms for $\theta = 15^\circ$ are shown below:

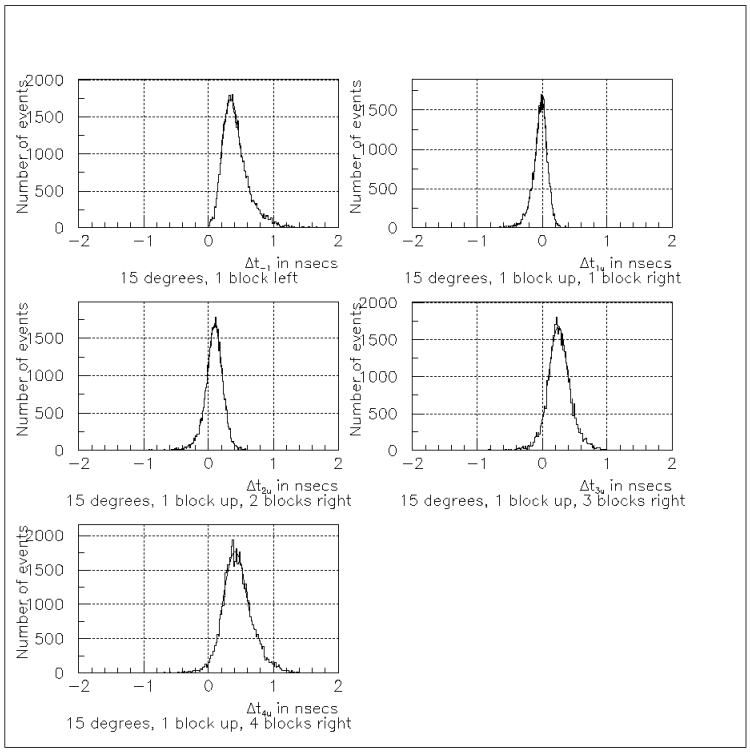

Figure 7

We apply a Gaussian fit on each histogram, and plot the means $\mu_b(\theta)$ of Gaussian fits on the histograms for each block against angle θ, using the standard deviations $\sigma_b(\theta)$ of the Gaussian fits to define the error bars. The following template was obtained:

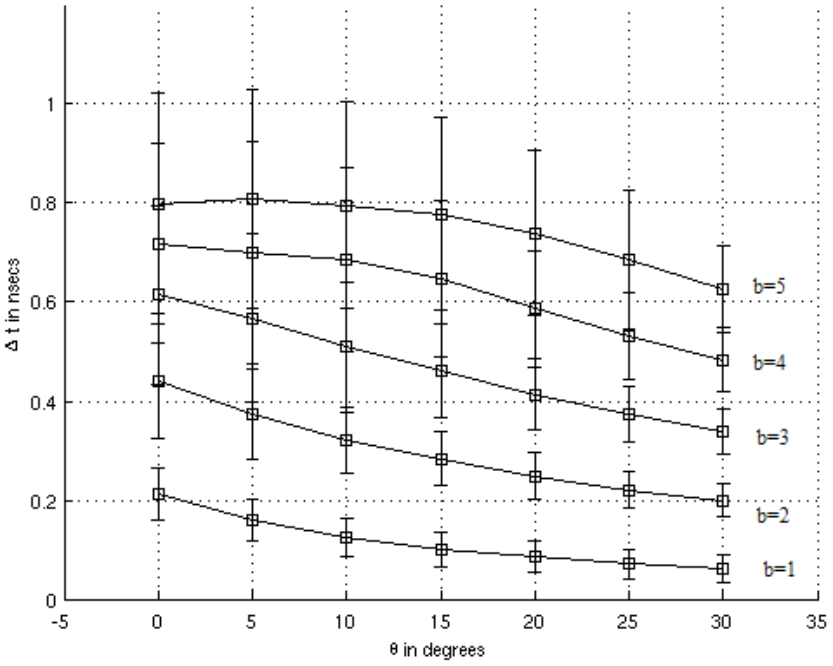
Δ t in nsecs
θ in degrees
b=5
b=4
b=3
b=2
b=1
0
0.2
0.4
0.6
0.8
1
-5
0
5
10
15
20
25
30
35

Figure 8

The tabular representation is given by:

Table 2: $\mu_b \pm \sigma_b$ of $\Delta t_b = t_b - t_{min}$

$\theta(^\circ)$	$\Delta t_m \pm \sigma$ in nsec in b=				
	1	2	3	4	5
0	0.21 ± 0.05	0.44 ± 0.12	0.62 ± 0.18	0.72 ± 0.20	0.80 ± 0.22
5	0.16 ± 0.04	0.37 ± 0.09	0.57 ± 0.17	0.70 ± 0.23	0.80 ± 0.22
10	0.13 ± 0.04	0.32 ± 0.07	0.51 ± 0.13	0.69 ± 0.19	0.80 ± 0.21
15	0.10 ± 0.04	0.28 ± 0.05	0.46 ± 0.09	0.65 ± 0.16	0.78 ± 0.20
20	0.09 ± 0.03	0.25 ± 0.05	0.41 ± 0.07	0.59 ± 0.12	0.74 ± 0.17
25	0.07 ± 0.03	0.22 ± 0.04	0.37 ± 0.06	0.53 ± 0.09	0.69 ± 0.14
30	0.06 ± 0.03	0.20 ± 0.03	0.34 ± 0.05	0.48 ± 0.07	0.63 ± 0.09

To maximize the accuracy of our method, we obtain also the means and variances of other blocks for which adequate information is available - that is, $E_b > 1$MeV in the majority of events. Thus the blocks we consider in our method are, the single block on the left of the minimum time block ($b = -1$), all blocks in the same row and to the right of the reference block ($b = 1, 2, \ldots$, and all blocks to the right and one row above the reference block ($b = 1u, 2u, \ldots$). These blocks are shaded in the diagram below:

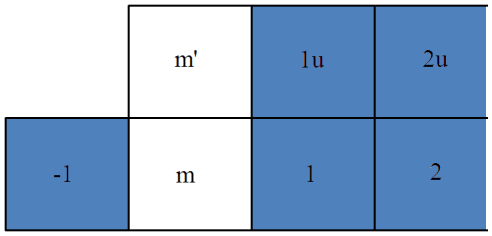

Figure 9

Note that for the blocks above the minimum time block m, we use the block m' directly above m as the reference block. This is to accomodate the incorporation of the vertical direction into analysis in future research. Using reference block m for the upper blocks would mix information for the vertical direction into that for the horizontal direction. The histograms for the added blocks may be found in Annex C. The corresponding table of means and standard deviations is as follows:

In addition to our graph in Figure 8, we now add two more graphs to our template:

Table 3: $\mu_b \pm \sigma_b$ of $\Delta t_b = t_b - t_m$ for $b = -1$ and $\Delta t_b = t_b - t_{m'}$ for the rest

$\theta(^\circ)$	$\Delta t_m \pm \sigma$ in nsec in b=				
	-1	1'	2'	3'	4'
0	0.21 ± 0.05	0.09 ± 0.08	0.27 ± 0.14	0.42 ± 0.19	0.51 ± 0.22
5	0.27 ± 0.08	0.05 ± 0.07	0.21 ± 0.12	0.37 ± 0.18	0.50 ± 0.21
10	0.31 ± 0.11	0.01 ± 0.07	0.15 ± 0.11	0.32 ± 0.15	0.46 ± 0.21
15	0.35 ± 0.15	-0.01 ± 0.08	0.10 ± 0.11	0.25 ± 0.14	0.41 ± 0.19
20	0.36 ± 0.17	-0.03 ± 0.10	0.06 ± 0.12	0.19 ± 0.14	0.35 ± 0.18
25	0.37 ± 0.17	-0.04 ± 0.12	0.03 ± 0.14	0.15 ± 0.15	0.29 ± 0.17
30	0.38 ± 0.17	-0.05 ± 0.13	0.01 ± 0.15	0.12 ± 0.16	0.23 ± 0.16

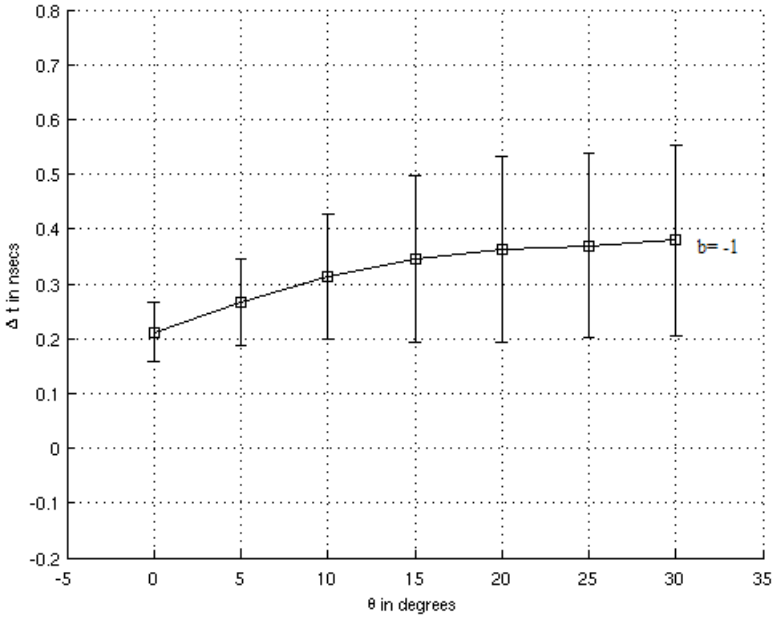

Figure 10

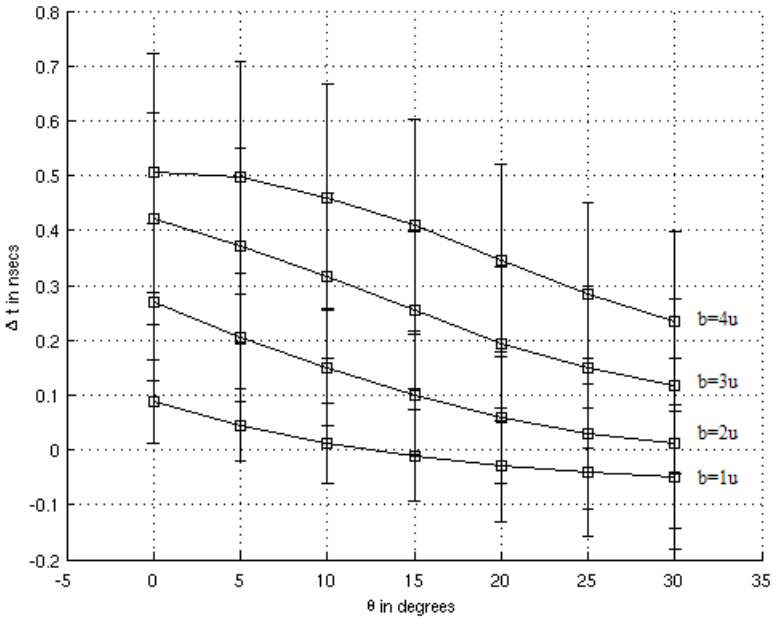

Figure 11

At this point, we recall that the time uncertainties involved so far have not taken into account the 100ps=0.1ns resolution of the timing instrument. Note that the resolution is on a similar scale as the σ_b's. To take into account the instrumental uncertainty, we add it to the statistical uncertainty in quadrature to obtain the total uncertainty

$$\sigma'_b = \sqrt{\sigma_b^2 + 0.1^2} \tag{2}$$

Now, given any event with unknown incident angle, we can compare the measured Δt_b's with the μ_b's and σ'_b's to make an informed guess at the angle. The next step is to find out how good this guess is.

4 Testing the Accuracy of the Method

We generate 10^5 events for each value of $\theta = 0°, 5°, \ldots, 30°$ on GEANT using a different randomization seed. For any given event, we obtain Δt_b for blocks with deposited energy exceeding 1MeV. For each angle ϕ in the template, we calculate the χ^2 statistic

$$\chi^2(\phi) = \frac{1}{n-1} \sum_{b:E_b>1MeV} \frac{(\Delta t_b - \mu_b(\phi))^2}{\sigma'^2_b(\phi)} \tag{3}$$

where n is the number of blocks with $E_b > 1MeV$

The value of ϕ that minimizes $\chi^2(\phi)$, giving χ^2_{min}, is the output ϕ_{out} of our algorithm. For each of the output angles ϕ_{out}, we bin the events with output ϕ_{out} according to their θ values. These histograms are listed in Annex D.

Obviously, the more $\phi_{out} = \theta$ events there are, the better our method. We note from Annex D that each of the peaks occurs at θ, as expected. However, we can improve the angular resolution further by considering the following:

For a given event, if the χ^2 values for different ϕ are very close to one another (in other words, the differences in χ^2 values are small compared to the magnitude of χ^2_{min}), the algorithm is likely to minimize to the wrong angle. For a given output ϕ_{out}, we create a scatterplot of χ^2_{min} against $\Delta\chi^2 = \chi^2_2 - \chi^2_{min}$ where χ^2_2 is the next smallest calculated value of $\chi^2(\phi)$. These scatterplots are listed in Annex E.

In each scatterplot, we separate the events into two categories. In the first category are events where $\phi_{out} = \theta$, which we mark in red. The second category contains events where $\phi_{out} \neq \theta$, which we mark in blue.

Referring to the scatterplots in Annex E, we note that for $\phi_{out} = 0°$ and $30°$, there are regions in which the density of blue dots is higher than the density of red dots. As expected, these blue dot regions occur where $\Delta\chi^2$ is small relative to χ^2_{min}. We delineate the abovementioned regions (using black solid lines in the scatterplots) and reject the events falling within these regions. Such regions are absent in the scatterplots for the other values of ϕ_{out}. For $0°$, the region is given by

$$\chi^2_{min} > 2.3\Delta\chi^2 + 0.8$$

and for $30°$ the region is given by

$$\begin{aligned} \chi^2_{min} &> 2\Delta\chi^2 + 1.1, \quad x < 0.5 \\ \chi^2_{min} &> 6.5\Delta\chi^2 - 1, \quad x \geq 0.5 \end{aligned}$$

With this additional step in place, the final results yielded by our algorithm are as shown in Annex F.

5 Interpretation of the Results

The resulting histograms show us the spread of possible θ values for each ϕ_{out}. We perform a Gaussian fit on each histogram, while fixing the mean at ϕ_{out}. These fits are displayed with the histograms in Annex F.

From each fit, we obtain the standard deviation $\sigma_{out}(\phi_{out})$ which we take to be the uncertainty of the angle found by our algorithm. We tabulate and graph the $\sigma_{out}(\phi_{out})$ values below:

Table 4: Error function for χ^2 minimization algorithm

$\phi_{out}(^\circ)$	0	5	10	15	20	25	30
$\sigma_{out}(^\circ)$	5.8 ± 0.4	8 ± 2	10 ± 2	9.0 ± 1.0	9.5 ± 0.9	9.00 ± 0.16	7.0 ± 0.5

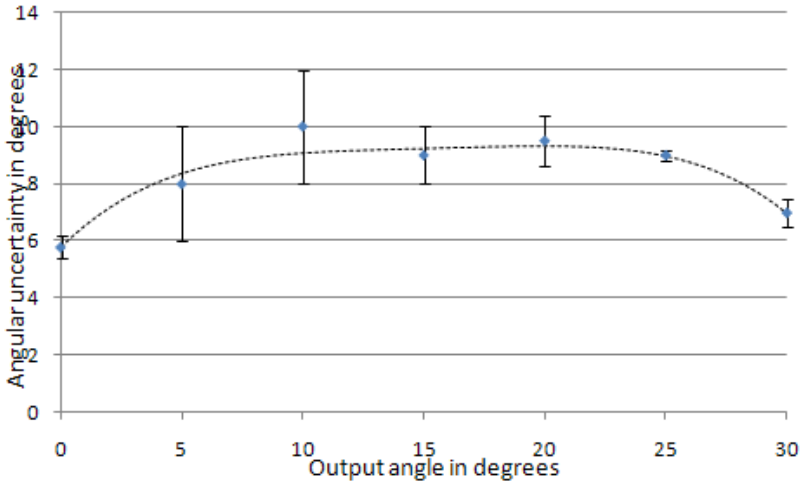

Figure 12

We fit a polynomial curve through the points and obtain

$$\sigma_{out} = (-5.64 \times 10^{-5})\phi_{out}^4 + (3.46 \times 10^{-3})\phi_{out}^3 - 0.0796\phi_{out}^2 + 0.838\phi_{out} + 5.80$$

The maximum residual is about 0.9, which we consider to be small relative to the σ_{out} values.

6 Conclusion

From the previous graph, we conclude that our proposed method yields angle measurements with uncertainties of no more than 10°. When two events are detected simultaneously in the calorimeter, measuring their incidence angles allows us to determine kinematic consistency as well as the decay vertex.

However, more needs to be done before we can perform such measurements. Our analysis was restricted along one dimension, whereas photons will be impinging on a two-dimensional surface in the actual experiment. Hence a study incorporating a vertical angle of incidence is required.

Moreover, the list of techniques and variables we tested in this project is not exhaustive and it is very likely that there exists another technique that would give better angular resolution using the same apparatus. Nevertheless, our upper bound of 10° on the 1-dimensional angular resolution (where previously no means of measuring the incidence angle could be employed) demonstrates

the usefulness of the new timing instrument and the potential benefits of further refinement on the angle measurement technique.

Annex A

Events binned by number of blocks (along center row) with deposited energy greater 1MeV. Each histogram corresponds to one angle. Note that the mode for each angle is 6. The least is 4, which is just slightly less than half the maximum number of blocks that may provide timing information.

Hence the threshold of 1MeV is justified. Setting a threshold higher than 1MeV would decrease the number of blocks providing information, while setting a lower threshold would decrease the time and energy resolution.

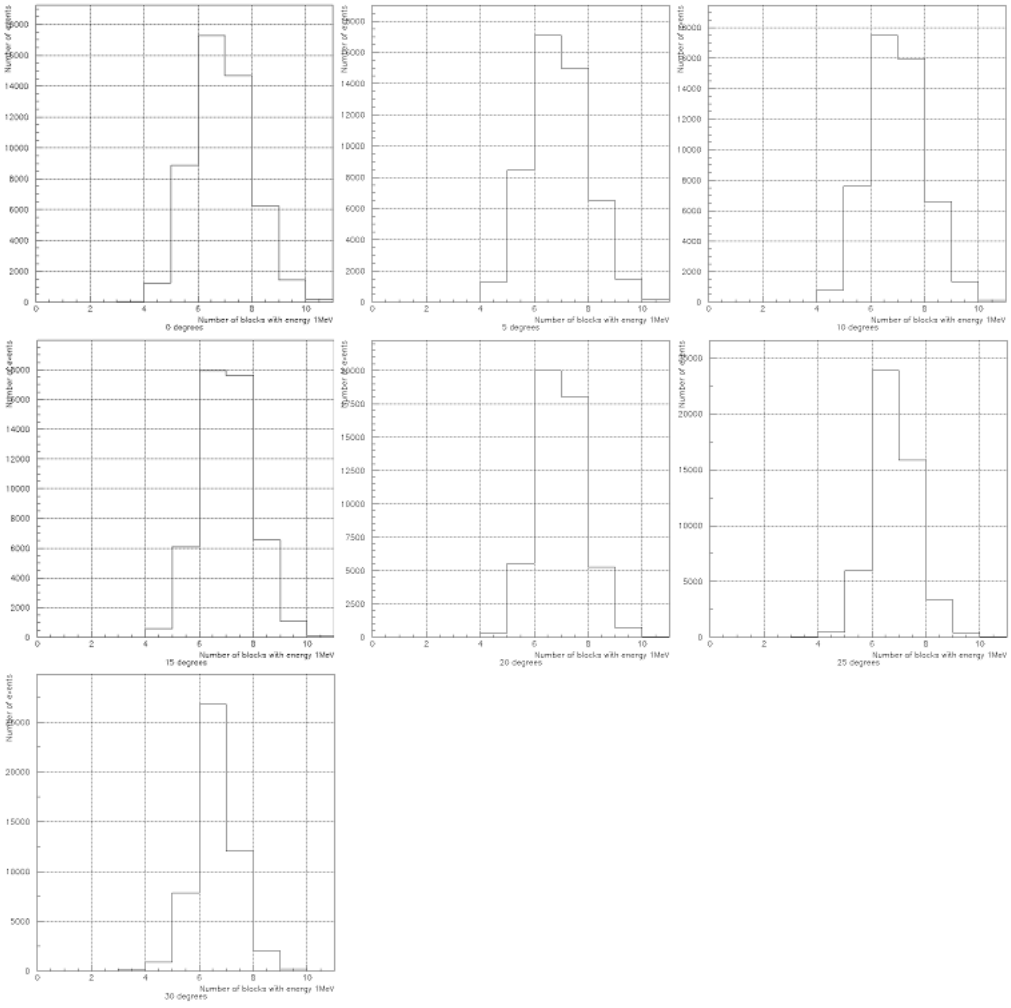

Figure A1

Annex B

Minimum time block as reference. Blocks to right of reference block.

The mean of the distribution increases as we move farther away from the reference block. Energy takes more time to accumulate to 1MeV due to attenuation over a longer distance. Since the distance travelled varies with angle, we expect the change in timing across the blocks to vary with angle as well.

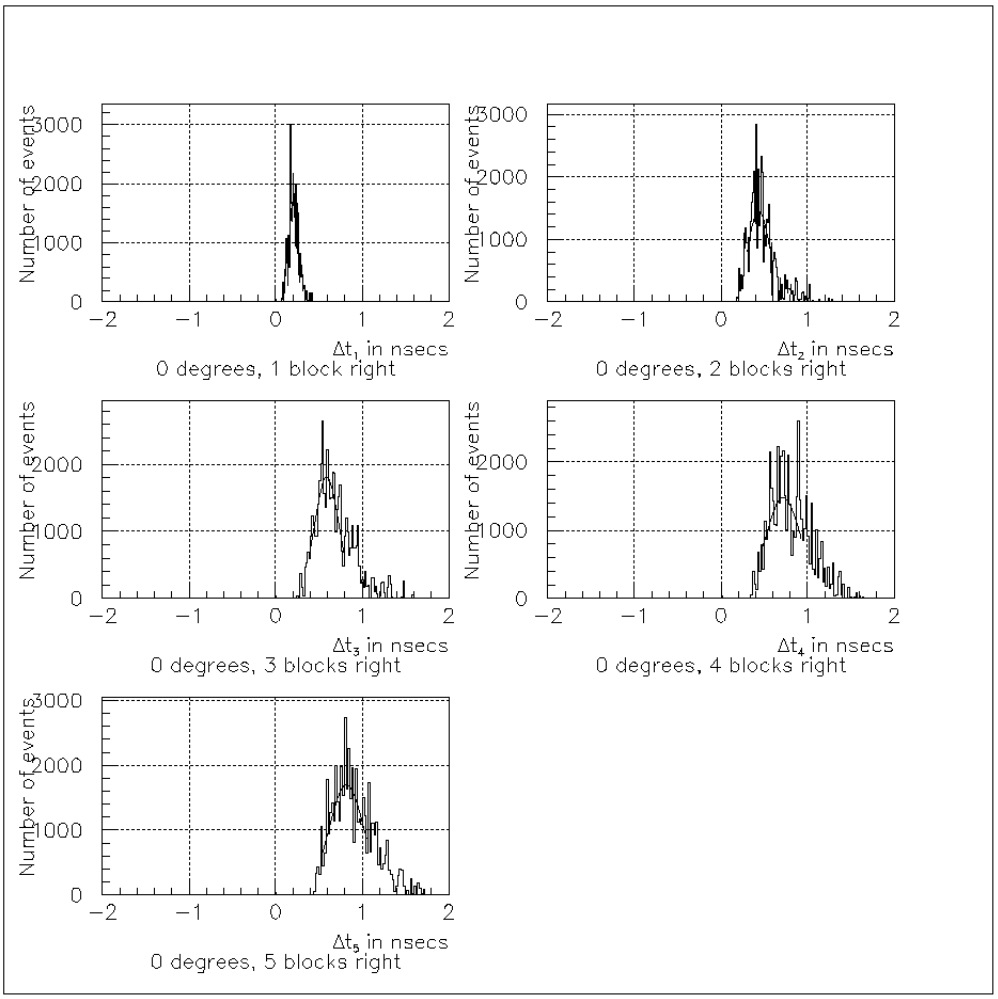

Figure B1

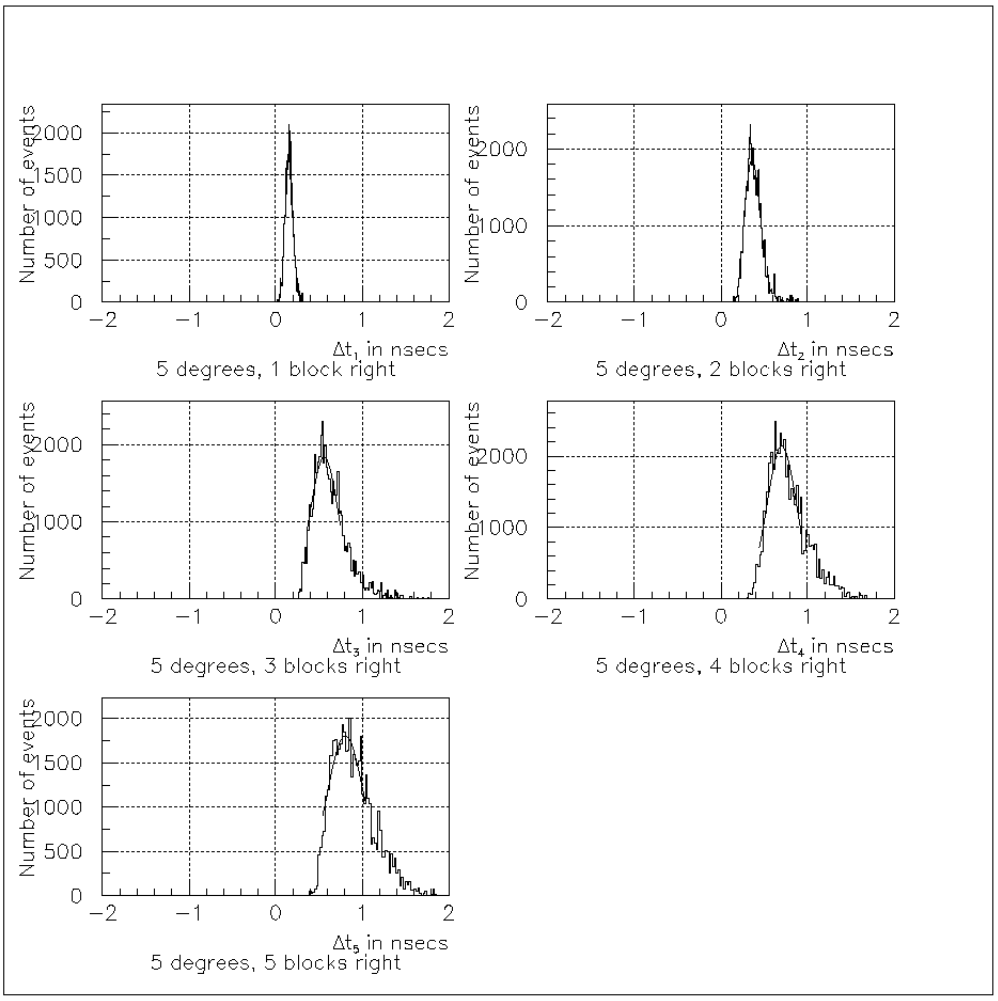
Number of events
2000
1500
1000
500
0
−2
−1
0
1
2
Δt1 in nsecs
5 degrees, 1 block right
Δt2 in nsecs
5 degrees, 2 blocks right
Δt3 in nsecs
5 degrees, 3 blocks right
Δt4 in nsecs
5 degrees, 4 blocks right
Δt5 in nsecs
5 degrees, 5 blocks right

Figure B2

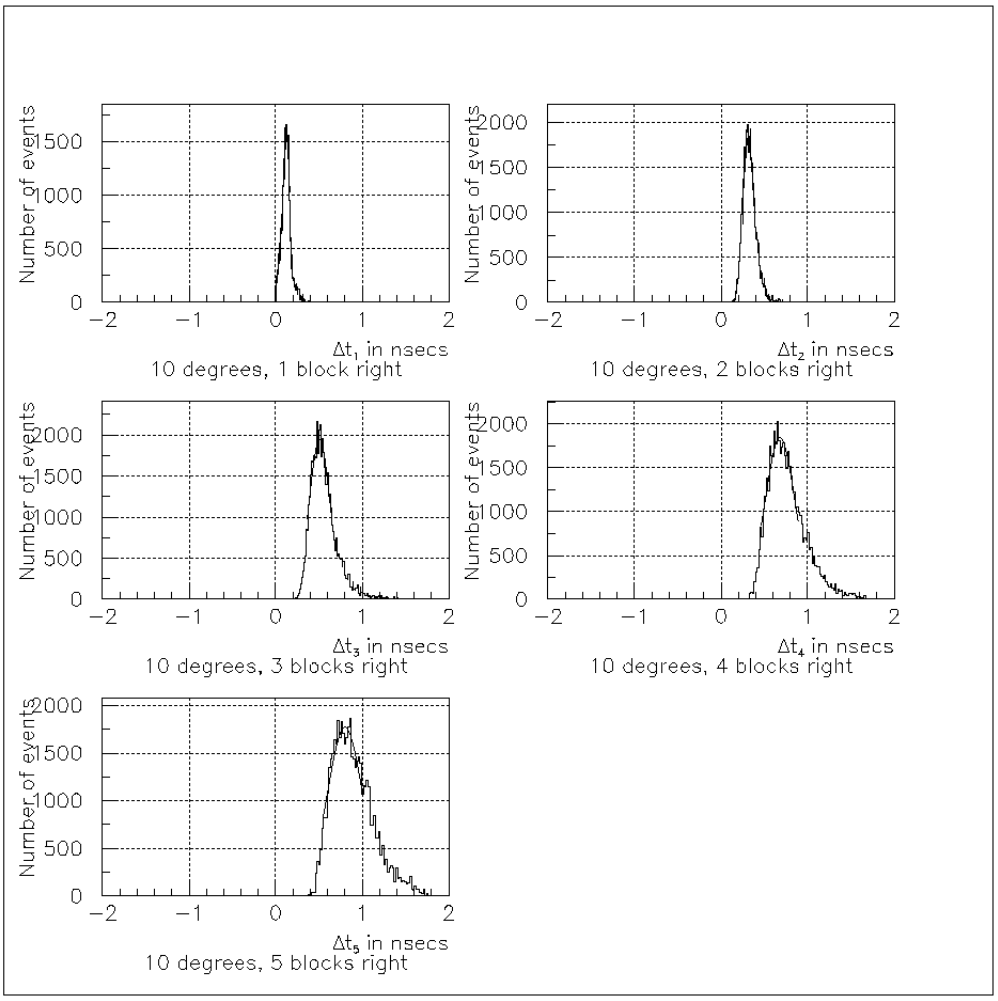
Number of events
Δt1 in nsecs
10 degrees, 1 block right
Number of events
Δt2 in nsecs
10 degrees, 2 blocks right
Number of events
Δt3 in nsecs
10 degrees, 3 blocks right
Number of events
Δt4 in nsecs
10 degrees, 4 blocks right
Number of events
Δt5 in nsecs
10 degrees, 5 blocks right

Figure B3

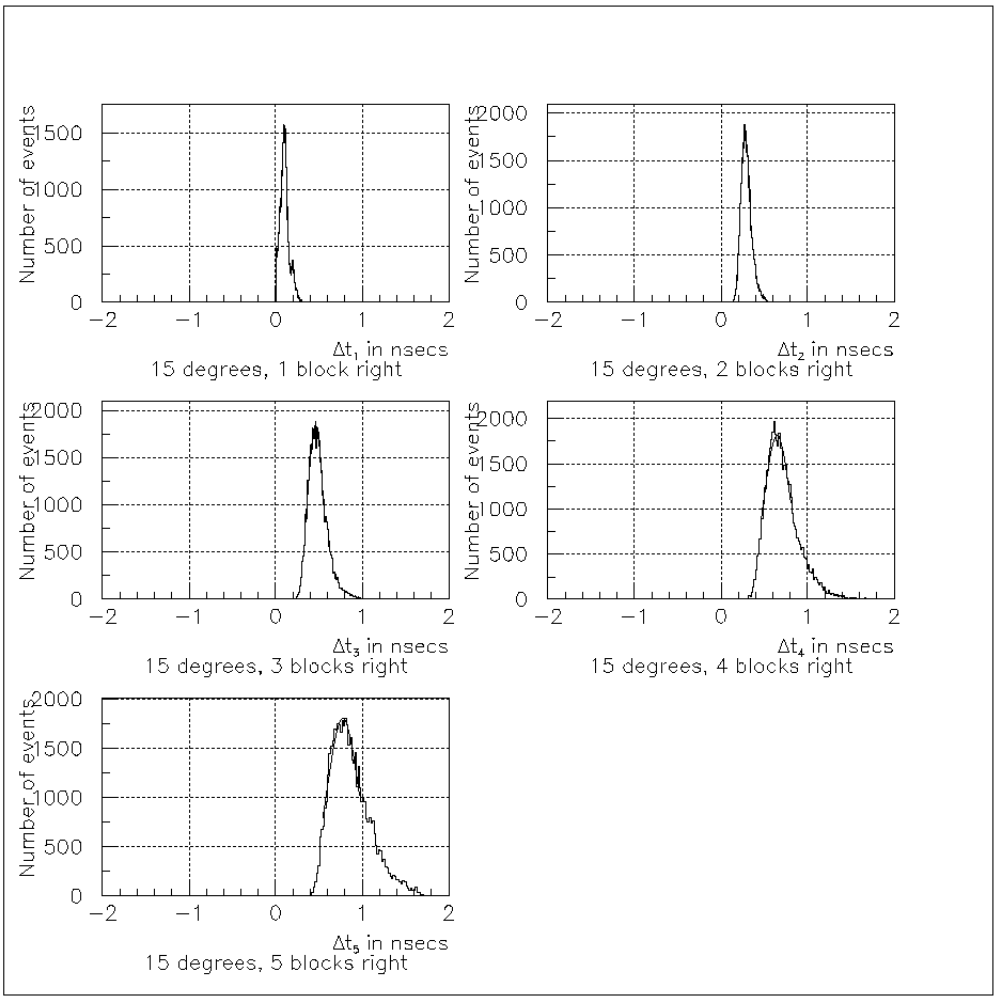
Number of events
Δt1 in nsecs
15 degrees, 1 block right
Δt2 in nsecs
15 degrees, 2 blocks right
Δt3 in nsecs
15 degrees, 3 blocks right
Δt4 in nsecs
15 degrees, 4 blocks right
Δt5 in nsecs
15 degrees, 5 blocks right

Figure B4

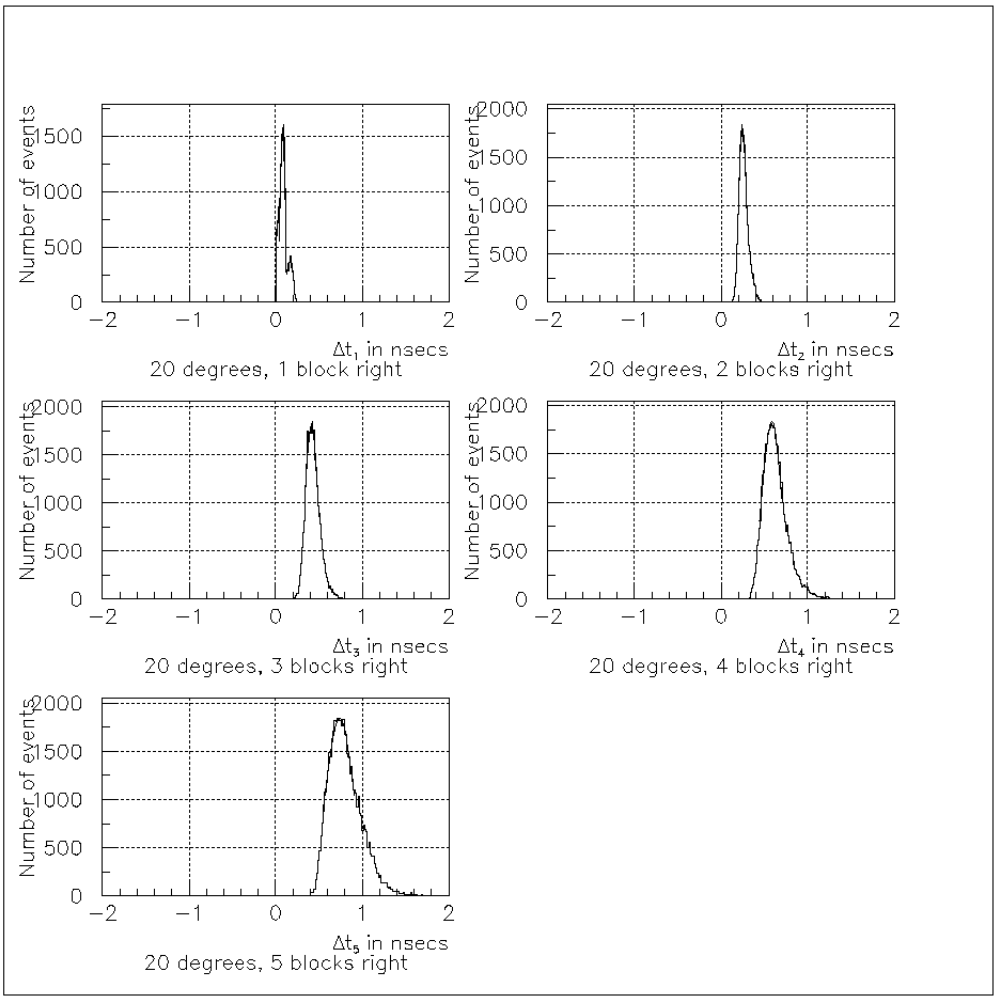
Number of events
2000
1500
1000
500
0
−2
−1
0
1
2
Δt1 in nsecs
20 degrees, 1 block right
Δt2 in nsecs
20 degrees, 2 blocks right
Δt3 in nsecs
20 degrees, 3 blocks right
Δt4 in nsecs
20 degrees, 4 blocks right
Δt5 in nsecs
20 degrees, 5 blocks right

Figure B5

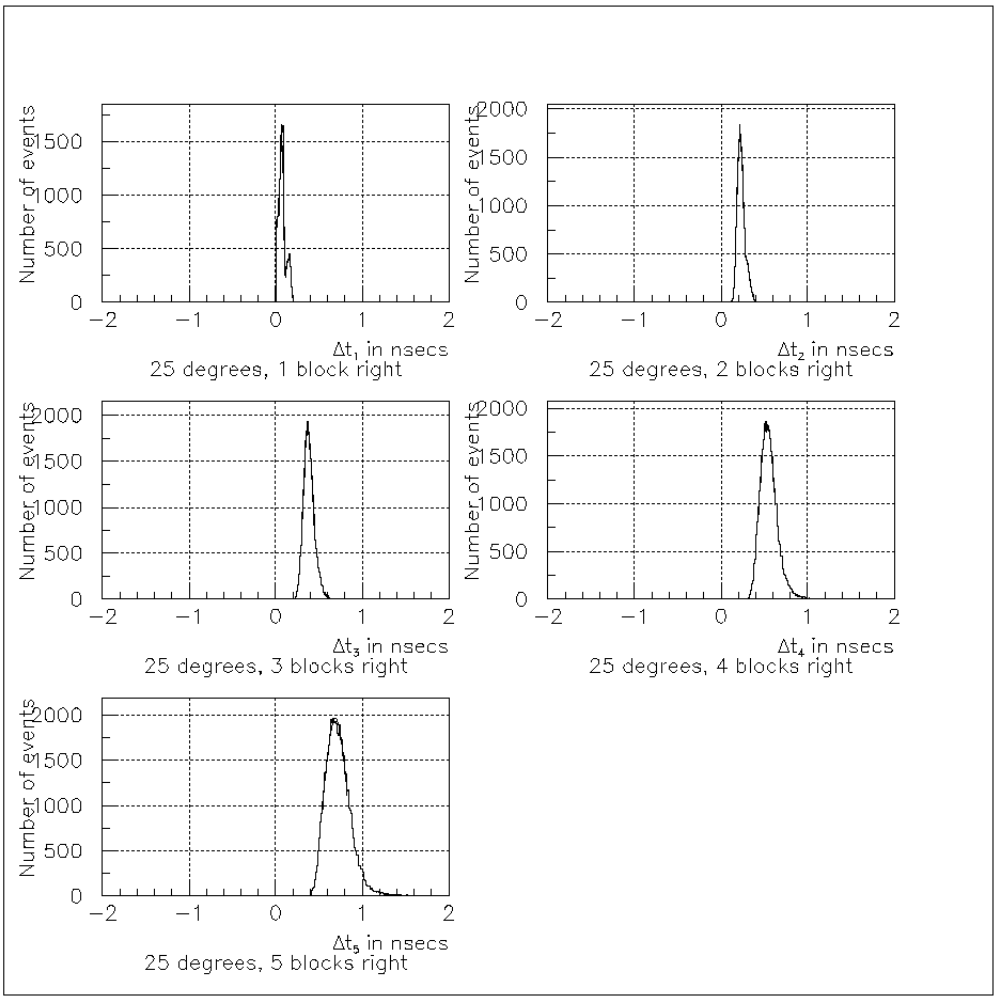
Number of events
Δt1 in nsecs
25 degrees, 1 block right
Δt2 in nsecs
25 degrees, 2 blocks right
Δt3 in nsecs
25 degrees, 3 blocks right
Δt4 in nsecs
25 degrees, 4 blocks right
Δt5 in nsecs
25 degrees, 5 blocks right

Figure B6

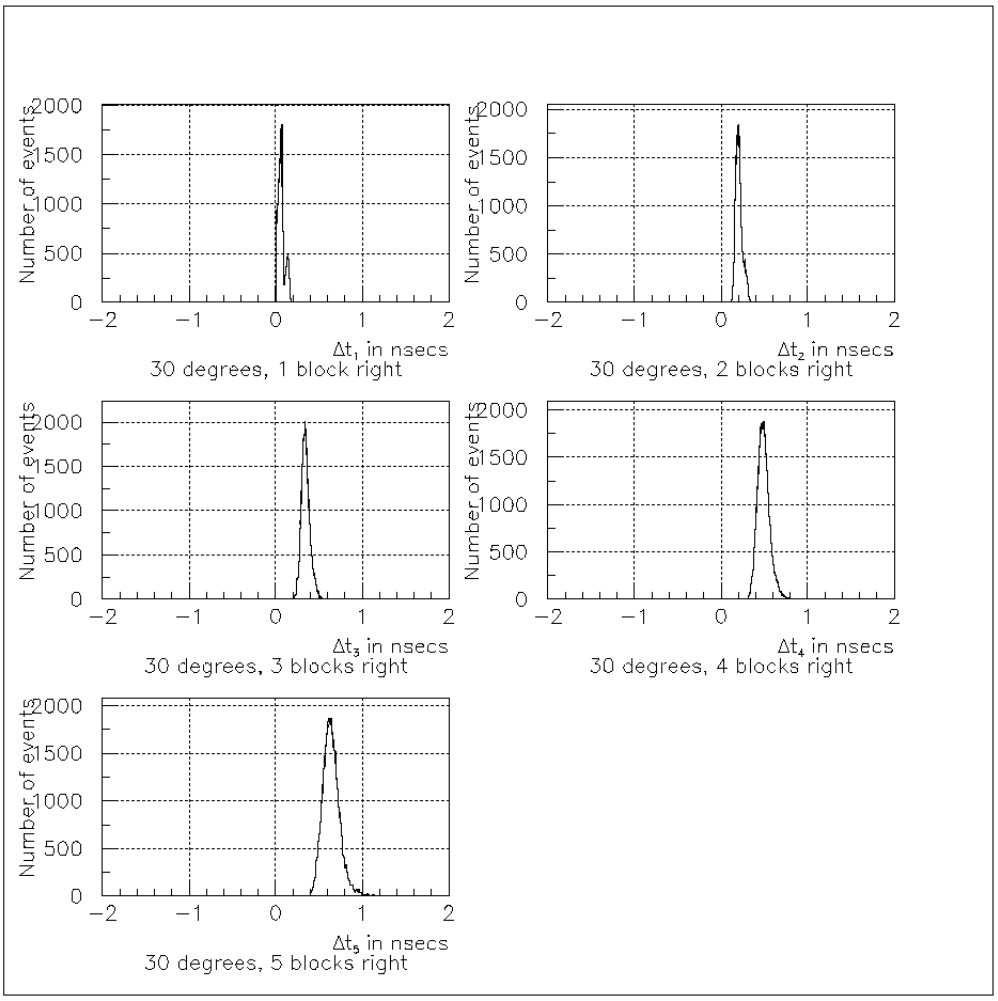
Number of events
2000
1500
1000
500
0
−2
−1
0
1
2
Δt1 in nsecs
30 degrees, 1 block right
Δt2 in nsecs
30 degrees, 2 blocks right
Δt3 in nsecs
30 degrees, 3 blocks right
Δt4 in nsecs
30 degrees, 4 blocks right
Δt5 in nsecs
30 degrees, 5 blocks right

Figure B7

Annex C

Minimum time block as reference. 1 block left of reference block ($b = -1$) and blocks one row above and to right of reference block ($b = 1u, 2u, \ldots, 4u$).

We note that the histograms for the blocks above and to the right of the reference block sometimes strays into the negative x-axis region. For events in this negative region, the rate of energy accumulation to the right is greater than that of the block directly above the minimum time block. This is possible because the incident photon has 0 degrees vertical angle, hence the energy flux towards the upper right may be greater than that directly upwards.

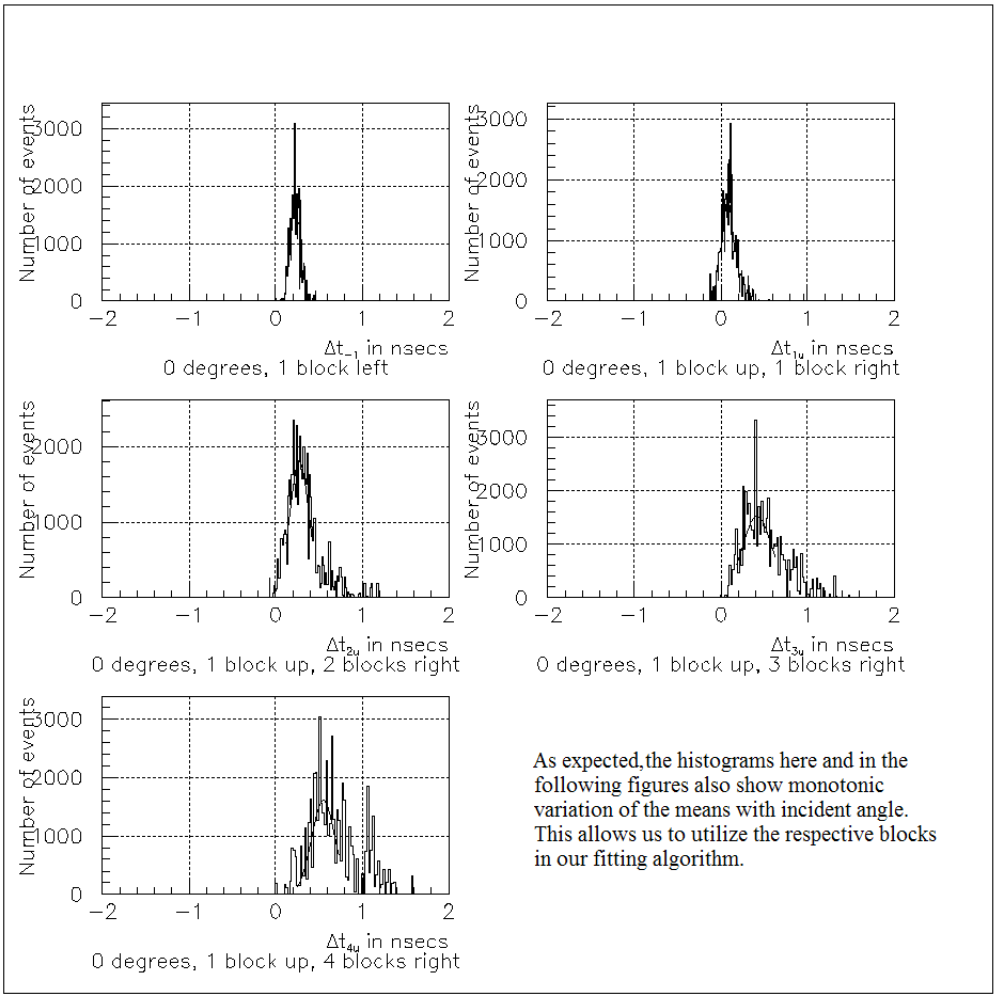

As expected, the histograms here and in the following figures also show monotonic variation of the means with incident angle. This allows us to utilize the respective blocks in our fitting algorithm.

Figure C1

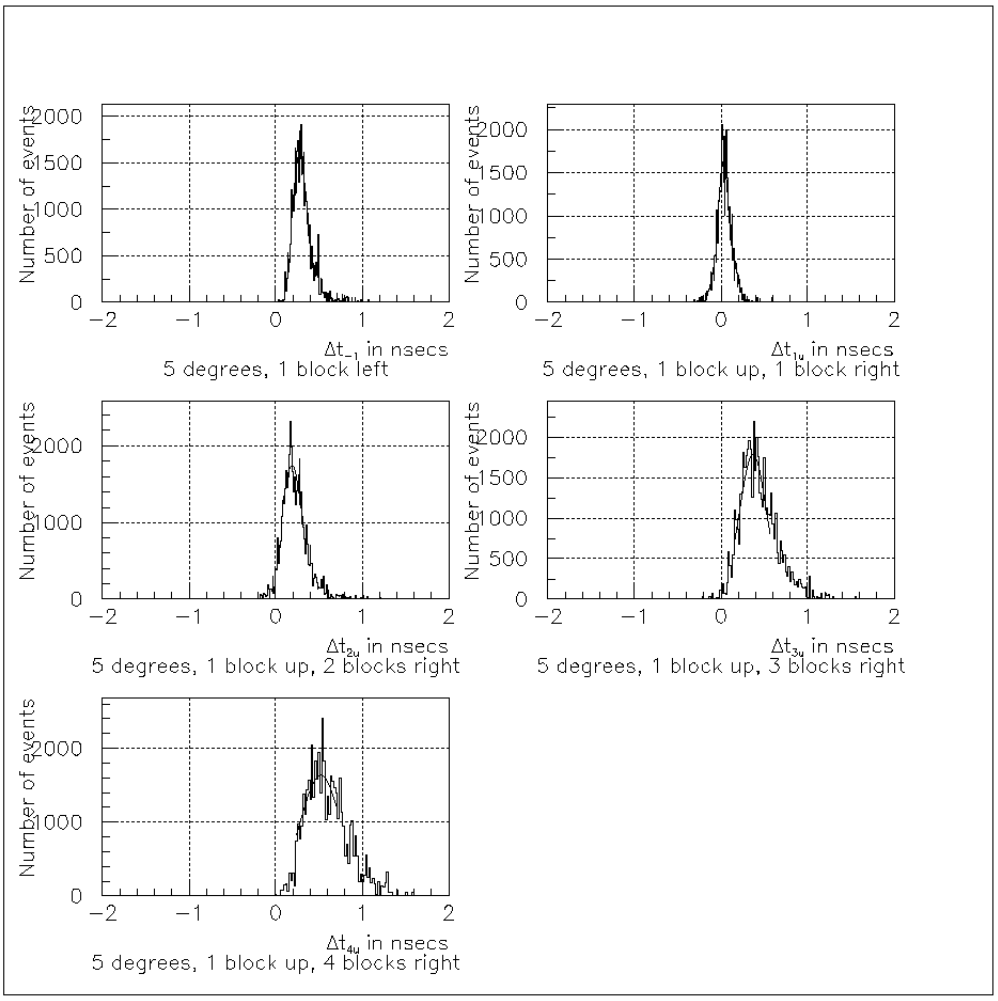
Number of events
2000
1500
1000
500
0
−2
−1
0
1
2
Δt−1 in nsecs
5 degrees, 1 block left
Δt1u in nsecs
5 degrees, 1 block up, 1 block right
Δt2u in nsecs
5 degrees, 1 block up, 2 blocks right
Δt3u in nsecs
5 degrees, 1 block up, 3 blocks right
Δt4u in nsecs
5 degrees, 1 block up, 4 blocks right

Figure C2

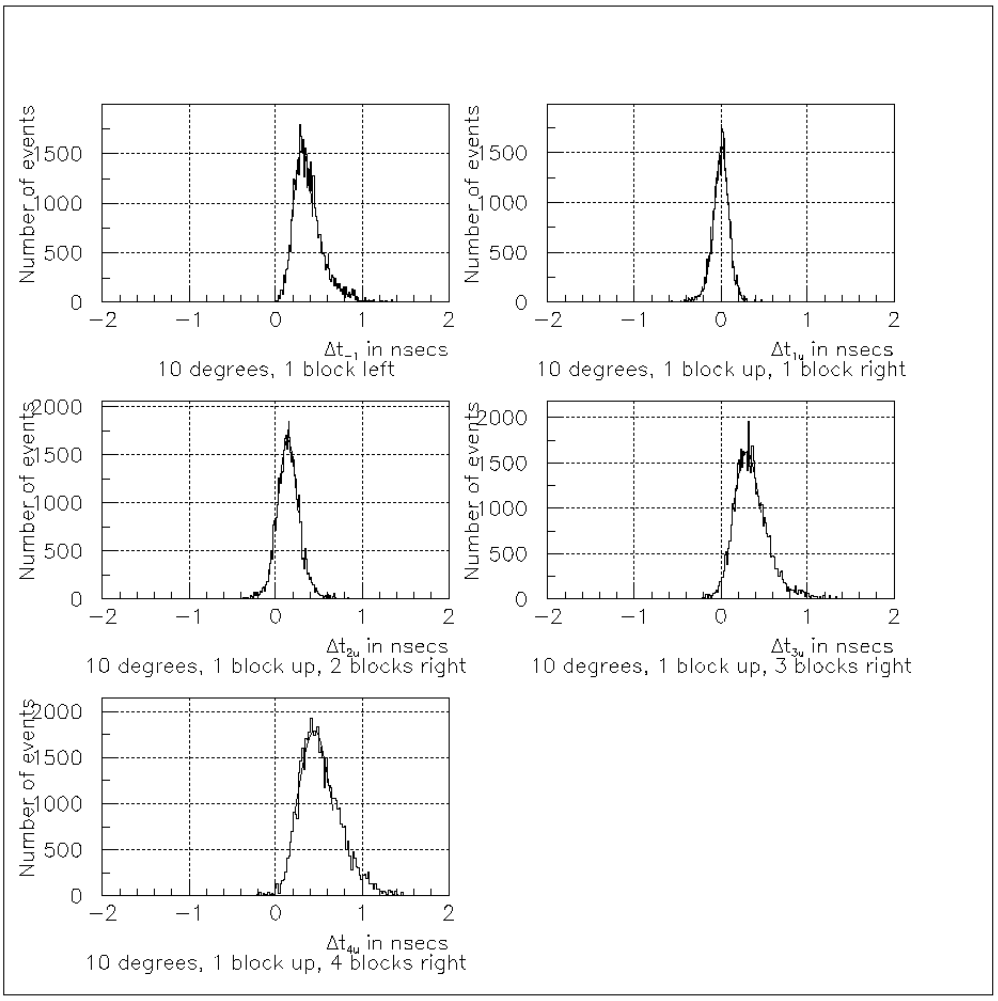
Number of events
Δt_-1 in nsecs
10 degrees, 1 block left
Number of events
Δt_1u in nsecs
10 degrees, 1 block up, 1 block right
Number of events
Δt_2u in nsecs
10 degrees, 1 block up, 2 blocks right
Number of events
Δt_3u in nsecs
10 degrees, 1 block up, 3 blocks right
Number of events
Δt_4u in nsecs
10 degrees, 1 block up, 4 blocks right

Figure C3

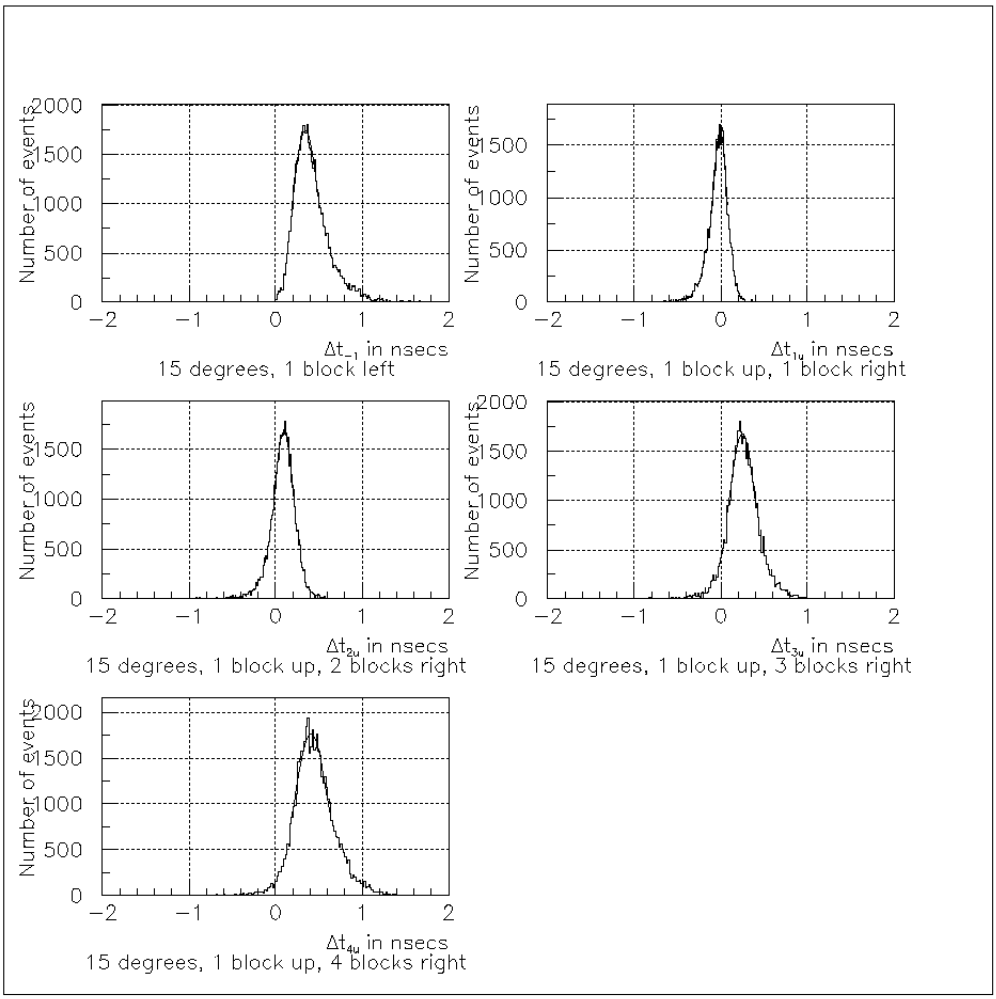
Number of events
2000
1500
1000
500
0
−2
−1
0
1
2
Δt−1 in nsecs
15 degrees, 1 block left
Δt1u in nsecs
15 degrees, 1 block up, 1 block right
Δt2u in nsecs
15 degrees, 1 block up, 2 blocks right
Δt3u in nsecs
15 degrees, 1 block up, 3 blocks right
Δt4u in nsecs
15 degrees, 1 block up, 4 blocks right

Figure C4

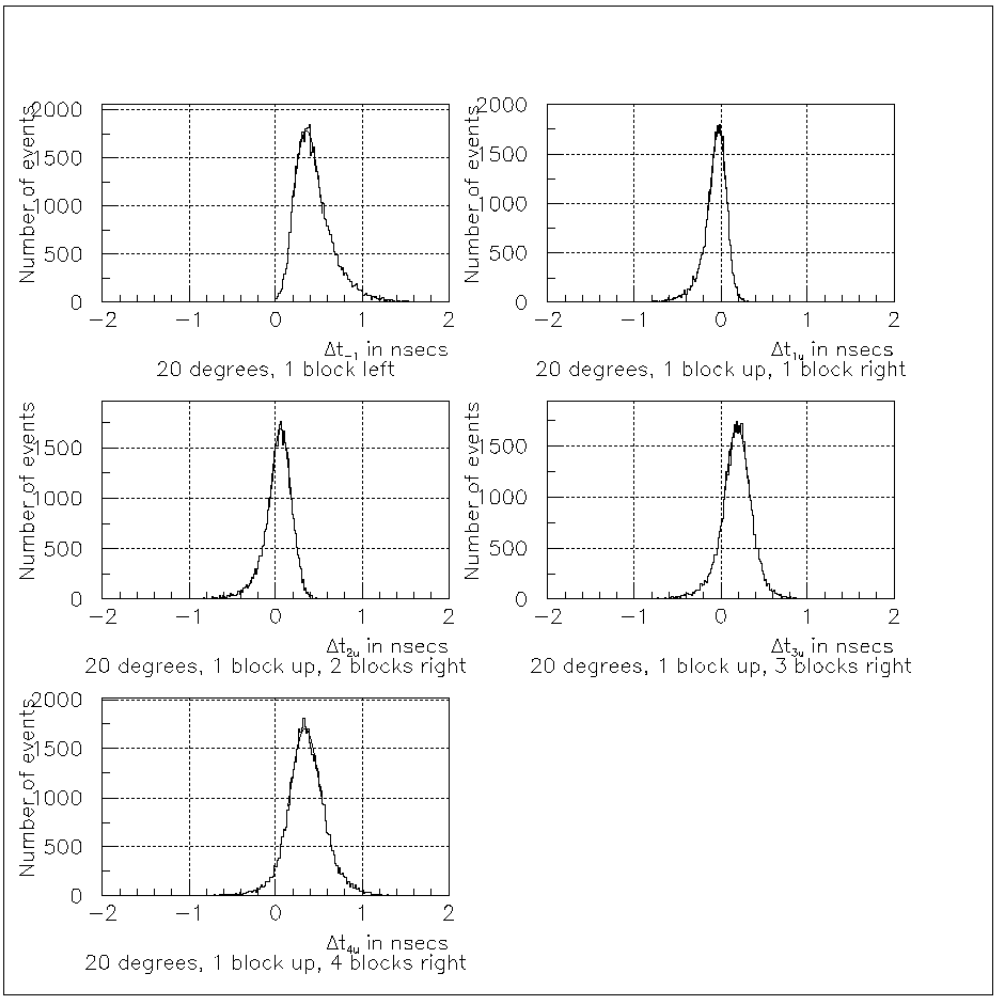
Number of events
2000
1500
1000
500
0
−2
−1
0
1
2
Δt−1 in nsecs
20 degrees, 1 block left
Δt1u in nsecs
20 degrees, 1 block up, 1 block right
Δt2u in nsecs
20 degrees, 1 block up, 2 blocks right
Δt3u in nsecs
20 degrees, 1 block up, 3 blocks right
Δt4u in nsecs
20 degrees, 1 block up, 4 blocks right

Figure C5

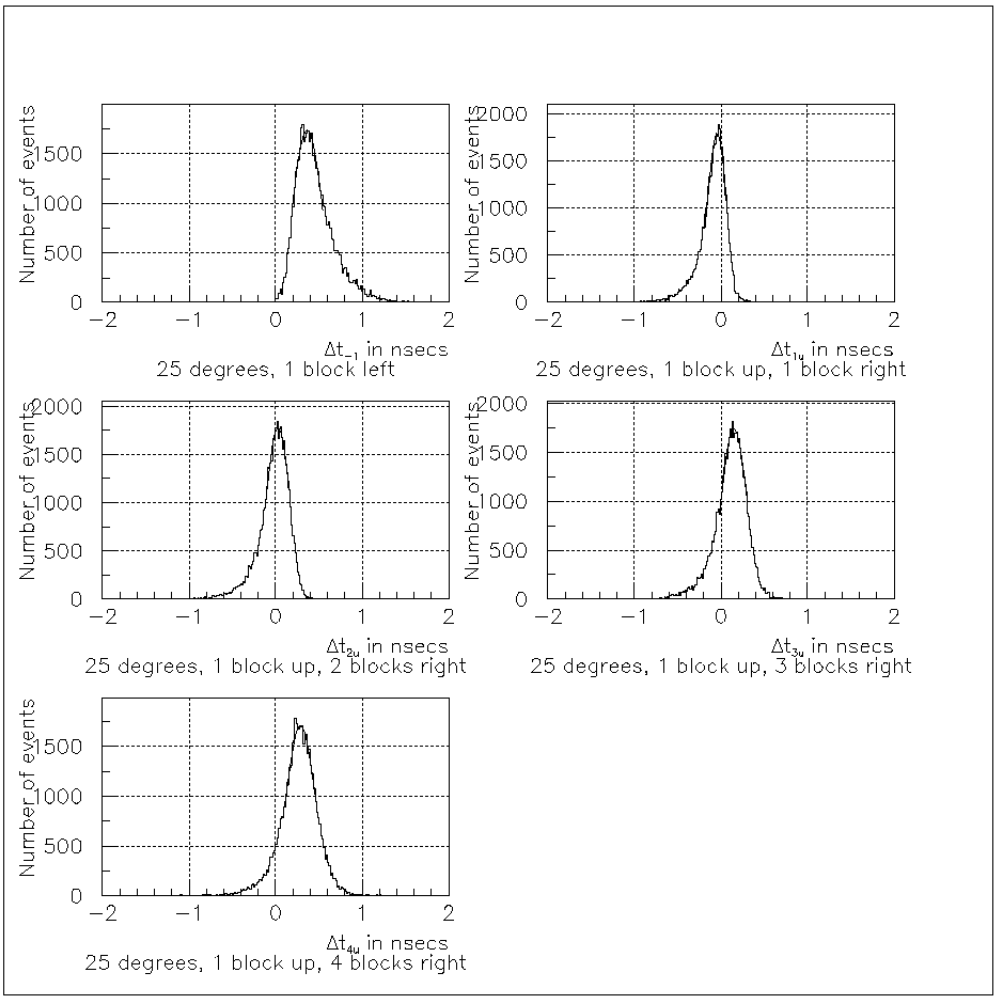
Number of events
0
500
1000
1500
2000
−2
−1
0
1
2
Δt_-1 in nsecs
25 degrees, 1 block left
Δt_1u in nsecs
25 degrees, 1 block up, 1 block right
Δt_2u in nsecs
25 degrees, 1 block up, 2 blocks right
Δt_3u in nsecs
25 degrees, 1 block up, 3 blocks right
Δt_4u in nsecs
25 degrees, 1 block up, 4 blocks right

Figure C6

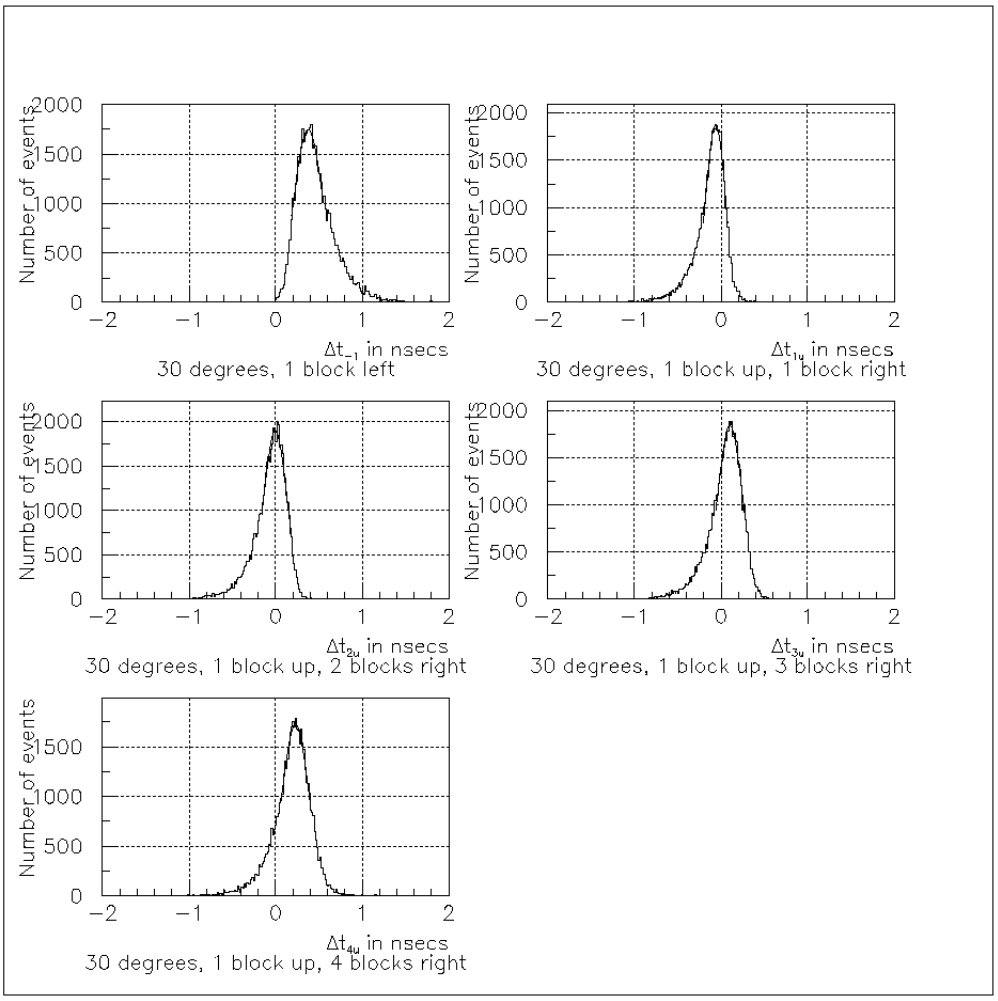
Number of events
2000
1500
1000
500
0
−2
−1
0
1
2
Δt_-1 in nsecs
30 degrees, 1 block left
Δt_1u in nsecs
30 degrees, 1 block up, 1 block right
Δt_2u in nsecs
30 degrees, 1 block up, 2 blocks right
Δt_3u in nsecs
30 degrees, 1 block up, 3 blocks right
Δt_4u in nsecs
30 degrees, 1 block up, 4 blocks right

Figure C7

Annex D

Output of fitting algorithm. Each histogram corresponds to one output angle, with x-axis as the input angle.

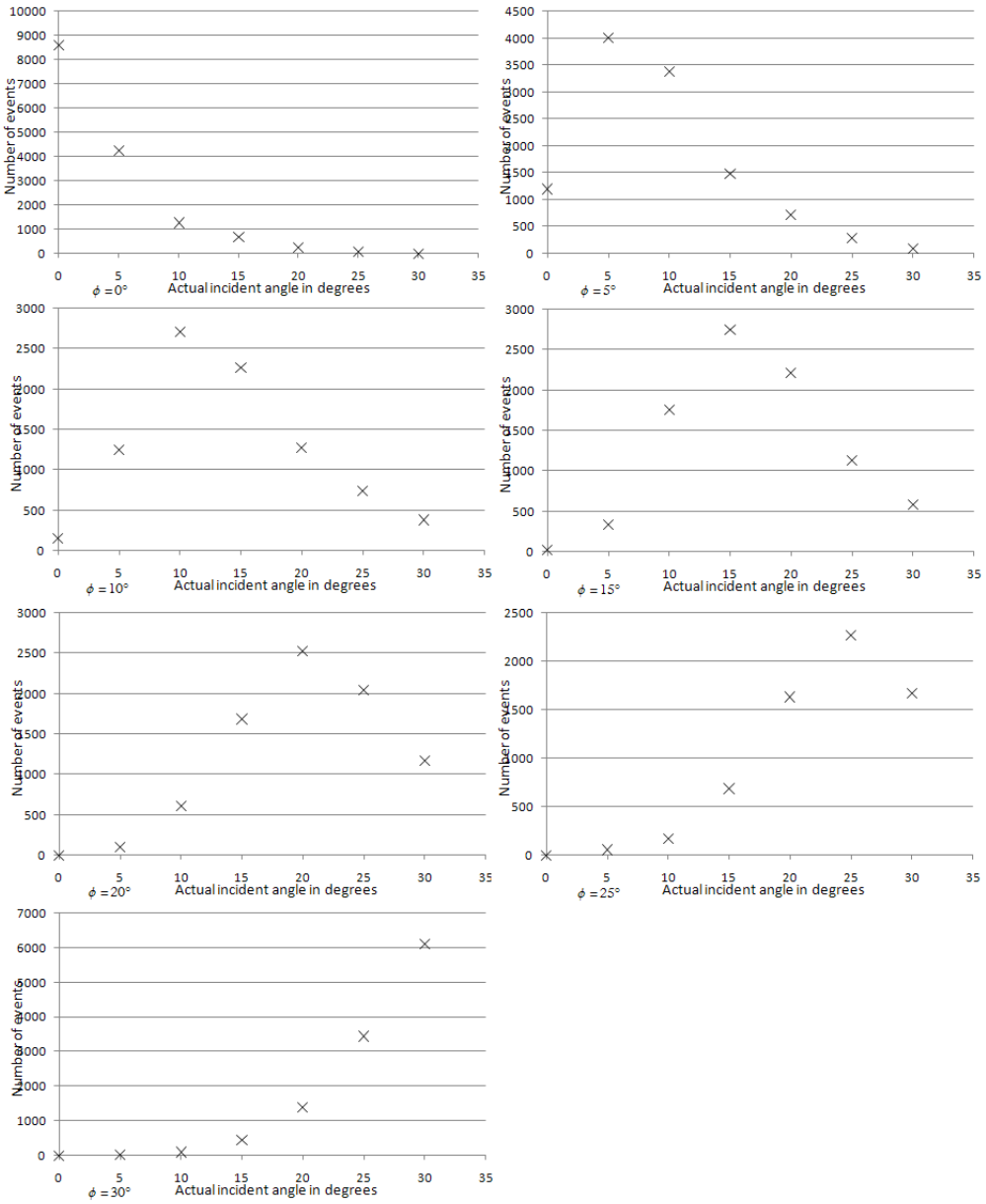

Figure D1

Annex E

Scatterplot of χ^2_{min} against $\Delta\chi^2$. Each scatterplot corresponds to one output angle.

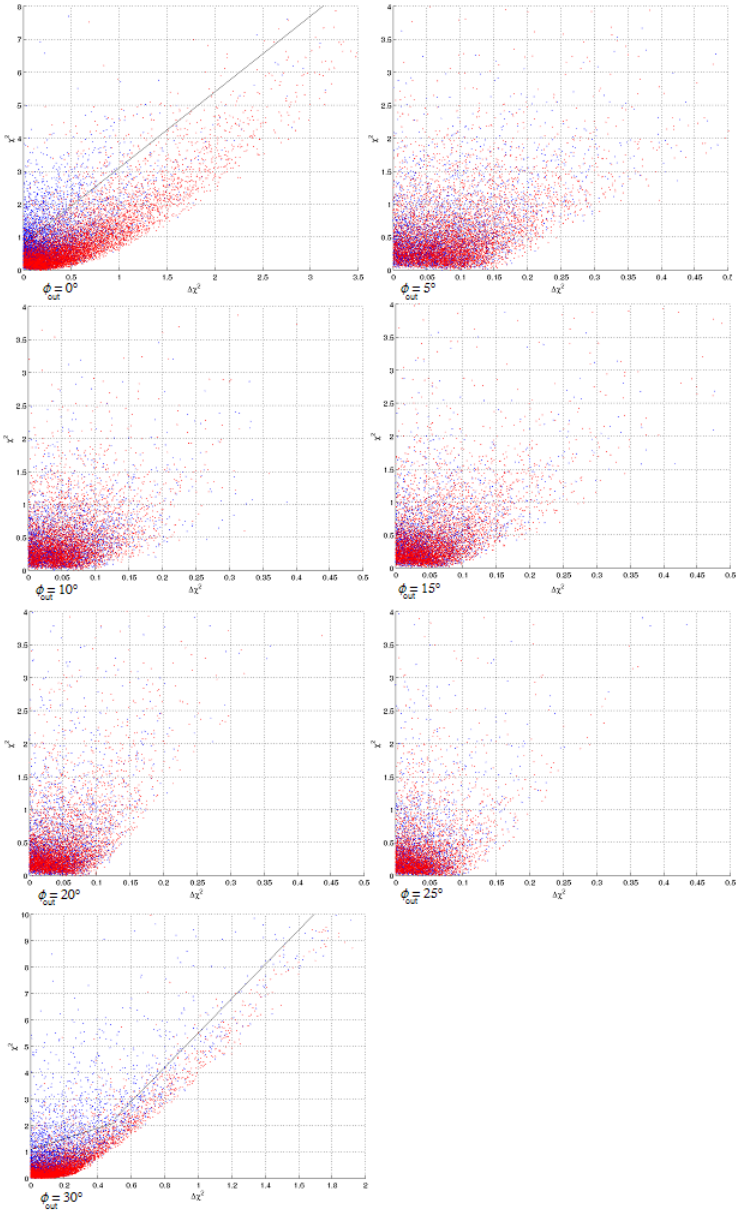

Figure E1

Annex F

Output of fitting algorithm and then correction subject to event categorization on $\chi^2_{min} - \Delta\chi^2$ criteria. Each histogram corresponds to one output angle with x-axis as input angle.

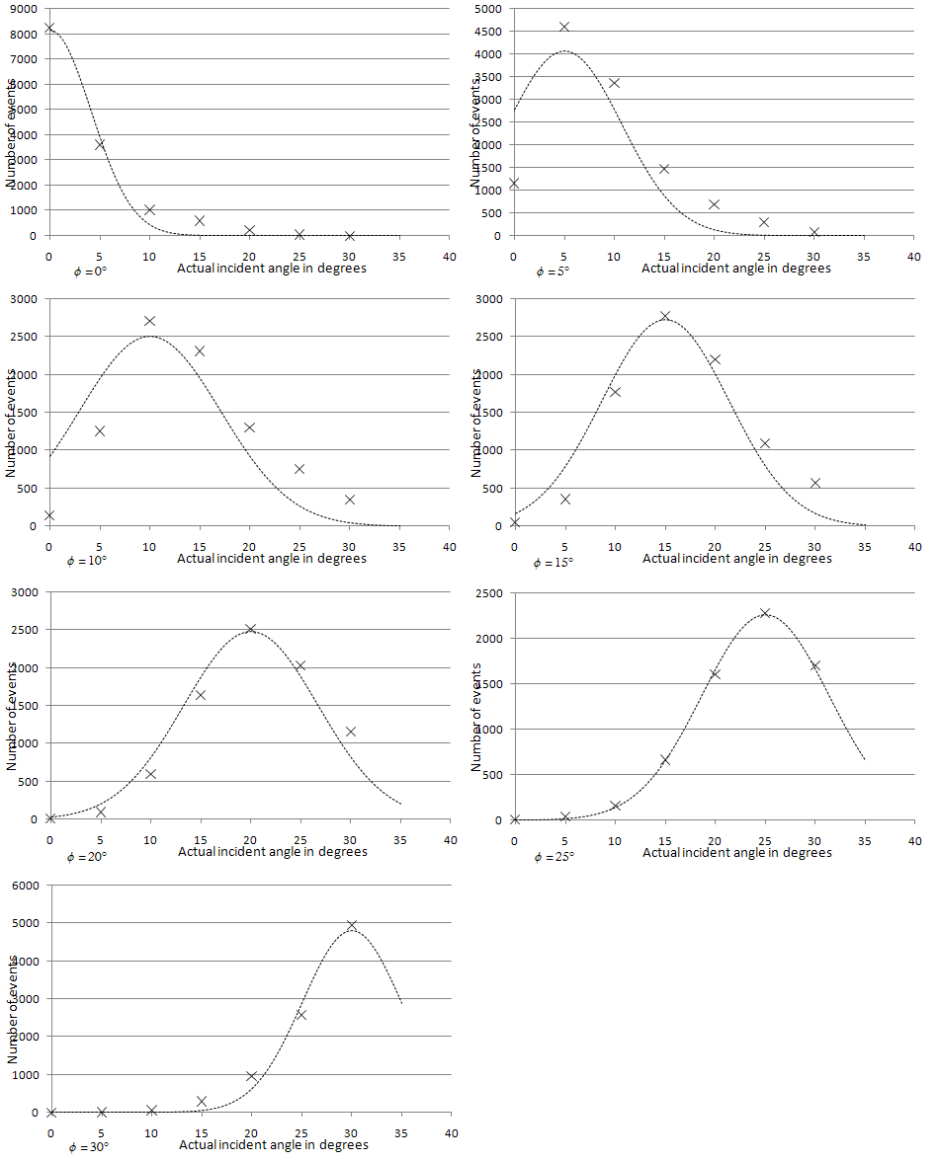

Figure F1

References

[1] Buras, A.J. et al. Waiting for precise measurements of $K^+ \to \pi^+\nu\overline{\nu}$ and $K_L^0 \to \pi^0\nu\overline{\nu}$. hep-ph/0405132, 2004.

[2] Perdue, Gabriel N. Search for the rare decay $K_L^0 \to \pi^0\nu\overline{\nu}$. PhD thesis, University of Chicago, 2008.

[3] Fernow, Richard C. *Introduction to Experimental Particle Physics*, pp. 25–6, Cambridge University Press, 1986.

[4] Application Software Group, Computing and Networks Division, CERN. GEANT–Detector Description and Simulation Tool. `http://wwwasdoc.web.cern.ch/wwwasdoc/geant_html3/geantall.html`, 1993.

[5] Weisstein, Eric W. "Central Limit Theorem." From MathWorld–A Wolfram Web Resource. `http://mathworld.wolfram.com/CentralLimitTheorem.html`, 2009.

[6] Scott, David W. On optimal and data-based histograms, *Biometrika*, 66:605-610.

[7] Perkins, Donald H. *Introduction to High Energy Physics*, pp. 44–5, Addison-Wesley Publishing Company, 1987.

[8] Groom, D.E. Atomic and Nuclear Properties of Materials. `http://pdg.lbl.gov/AtomicNuclearProperties/`, 2007.